Stochastic Fusion Simulations and Experiments Suggest Passive and Active Roles of Hemagglutinin during Membrane Fusion

Donald W. Lee, Vikram Thapar, Paulette Clancy, and Susan Daniel*
School of Chemical and Biomolecular Engineering, Cornell University, Ithaca, New York

ABSTRACT Influenza enters the host cell cytoplasm by fusing the viral and host membrane together. Fusion is mediated by hemagglutinin (HA) trimers that undergo conformational change when acidified in the endosome. It is currently debated how many HA trimers, w, and how many conformationally changed HA trimers, q, are minimally required for fusion. Conclusions vary because there are three common approaches for determining w and q from fusion data. One approach correlates the fusion rate with the fraction of fusogenic HA trimers and leads to the conclusion that one HA trimer is required for fusion. A second approach correlates the fusion rate with the total concentration of fusogenic HA trimers and indicates that more than one HA trimer is required. A third approach applies statistical models to fusion rate data obtained at a single HA density to establish w or q and suggests that more than one HA trimer is required. In this work, all three approaches are investigated through stochastic fusion simulations and experiments to elucidate the roles of HA and its ability to bend the target membrane during fusion. We find that the apparent discrepancies among the results from the various approaches may be resolved if nonfusogenic HA participates in fusion through interactions with a fusogenic HA. Our results, based on H3 and H1 serotypes, suggest that three adjacent HA trimers and one conformationally changed HA trimer are minimally required to induce membrane fusion ($w = 3$ and $q = 1$).

INTRODUCTION

Membrane fusion is an important process that enveloped viruses such as influenza use to enter host cells. The surface of influenza viruses contains hemagglutinin (HA) proteins that govern both the attachment of the virus to sialic acid receptors on a host cell and the fusion of the viral envelope with the host membrane. The HA protein is a trimer of three monomers; this protein unit will be referred to as an HA trimer. Below a pH of 5.8 (1), HA trimers can undergo conformational changes that insert hydrophobic fusion peptides into the target membrane to initiate membrane fusion (2). Despite extensive research on the fusion mechanism, the minimum number of HA trimers needed for fusion is still a matter of debate. In this work, we use simulations and experiments to resolve the possible roles of hemagglutinin in fusion.

Adopting the notation used by Bentz (3), we refer to the minimum number of HA trimers that are required for fusion as w, and the minimum number of HA trimers within the subset of w that must undergo conformational change as q. A direct way of determining w and q would be to observe distinct HA trimers inducing fusion in real time, but, as of this writing, such experiments are not yet possible. Therefore, w and q are extracted indirectly through the analysis of the kinetics of HA-induced membrane fusion, combined with electron-micrograph (EM) images (4–7) and crystallographic data (8–10) of intermediate states of membrane fusion. The general techniques used to study membrane fusion kinetics are discussed in Struck et al. (11) and Otterstrom and van Oijen (12). The kinetic data are often collected as a distribution of lag times between the acidification of HA trimers and the membrane fusion event, which is normally detected through the dequenching of membrane fluorophores. In past studies, different values for w and q were proposed depending on the experimental systems used to obtain the lag-time distributions and the statistical models used to interpret the data. Additionally, many past studies did not assume that w and q can have different values. Generally, values of w or $q > 1$ suggest that multiple HA trimers act cooperatively to induce fusion, whereas a value of 1 suggests HA trimers do not act cooperatively to induce fusion. Past studies have provided evidence for both cooperative and noncooperative behavior of HA trimers to induce fusion, which appears to be contradictory. Through simulations and the analysis of kinetic data, we propose that contradictory observations can be reconciled if conformationally changed HA trimers play an active role in fusion whereas unchanged HA trimers play a passive role.

Variations in approaches that have led to different conclusions for w and q

There are three common approaches for determining w and q using kinetic data from fusion experiments:

One approach is to monitor how the fusion lag times change as the ratio between the number of fusogenic HA trimers ($HA_{1,2}$) and nonfusogenic HA trimers (HA_0) is varied while the total HA density is kept constant. This method is referred to as the "Variable F" approach by Imai et al. (13) because the fusion (F) capacity of virions (or virosomes) is

Submitted April 12, 2013, and accepted for publication December 6, 2013.

*Correspondence: sd386@cornell.edu

Donald W. Lee and Vikram Thapar contributed equally to this work.

Editor: Lukas Tamm.

0006-3495/14/02/0843/12 $2.00

http://dx.doi.org/10.1016/j.bpj.2013.12.048

being varied and not their binding (B) capacity. The fusion rate, V, can then be extracted from the slope of the cumulative lag-time distribution. Considering the fusion event as a reaction, an nth-order reaction equation such as $V = k[HA_{1,2}]^n$ could be used to correlate V with the number of cooperating HA trimers, n. Note that many past studies did not consider w and q as separate values, hence, n is considered as being either w or q ($n = w$ or q). Most kinetic data from the Variable F approach (13–16) support that HA trimers do not act cooperatively to induce fusion ($n = 1$).

A second approach, is to find the correlation between fusion rate and the total concentration of HA trimers, all of which are fusogenic ($HA_{1,2}$). This method is referred to as the "Variable FB" (13), Most results from past studies that used this approach (3,13,17–19) show that the fusion rate scales nonlinearly with fusogenic HA density, which indicates that HA trimers act cooperatively to induce fusion ($n > 1$).

A third approach, deduces n by analyzing the shape of the lag-time distribution obtained at a constant fusogenic HA density. This method is referred to as the "Constant FB" approach since the fusion and binding capacities of the virions (or virosomes) are not varied, though environmental conditions such as the pH to trigger fusion can be varied. Often, statistical models with n as the fitting parameter are used to fit the lag-time distribution. This approach usually concludes that n is >1 (3,19–25). Table S1 in the Supporting Material provides an extended summary of related works, along with their concluded values of w or q.

The work by Imai et al. (13) demonstrates that fusion kinetics proves sensitive to different approaches, despite the fact that the experimental system is otherwise the same. The Variable F approach suggests n is 1, whereas the Variable FB approach suggests n is >1. Because Imai et al. (13) did not consider that w and q can have different values, one value for n had to be chosen between the Variable F and FB results. They decided $n = 1$ according to the Variable F approach. However, we show that both of their results are consistent with each other if we allow w and q to take different values ($w \neq q$). The interpretation that w and q are not equal is that fusion proceeds through the involvement of both conformationally changed and unchanged HA trimers.

We present a mechanistic model and simulation strategy that can generate kinetic data showing both cooperative and noncooperative behaviors of HA trimers in inducing fusion when w is 3 and q is 1. The results for w and q were validated using kinetic data from both the experiments of Imai et al. (13) and our own fusion experiments, which studied the membrane fusion behavior of the H1 and H3 serotypes of HA trimers, respectively. We note here that the obtained values for w and q may not extend across other experimental systems that use different HA serotypes or fusion conditions.

In addition to extracting w and q from kinetic data, our model is able to capture the dependence of fusion lag times on target membrane properties, as shown by other works (26–28). Our model is notably different from other simulation models (19,24,25), which do not generate kinetic data that agree with the data from all three approaches and do not explicitly consider how target membrane properties affect fusion.

EXPERIMENT METHODS

Influenza virus labeling

To label the viral envelope with a fluorescent fluorophore, 5 μL of X31 A/Aichi/68 H3N2 (Charles River, Wilmington, MA) at a concentration of 2 mg/mL, along with 0.1 μL of 1.8 mM octadecyl rhodamine B chloride (R18; Invitrogen, Carlsbad, CA) in ethanol, and 250 μL of MES buffer (1 mM 2-(*n*-morpholino)ethanesulfonic acid, 150 mM NaCl, pH 7), were mixed in a vial for 1 h at room temperature using a water sonicator bath. Unincorporated R18 fluorophores were removed from solution using a G25 Sephadex spin column (GE Healthcare Biosciences, Pittsburgh, PA). The filtered virus solution was diluted in MES buffer by 10-fold before use.

Target bilayer compositions

DOPC (1,2-dioleoyl-*sn*-glycero-3-phosphocholine), POPC (1-palmitoyl-2-oleoyl-*sn*-glycero-3-phosphocholine), LPC (1-stearoyl-2-hydroxy-*sn*-glycero-3-phosphocholine), and cholesterol (Avanti Polar Lipids, Alabaster, AL) were individually dissolved in chloroform. The sialic acid receptor, G_{D1a} (Sigma-Aldrich, St. Louis, MO), was dissolved in a 2:1 chloroform/methanol solution. Oregon Green DHPE (Invitrogen), an acid-sensitive membrane fluorophore, was dissolved in ethanol. Two different lipid compositions were then prepared, labeled as compositions A and B. Composition A was prepared by mixing lipid components at a molar ratio of 4:4:2:0.1:0.001 DOPC/POPC/Cholesterol/G_{D1a}/Oregon Green DHPE, and composition B was prepared similarly, but with LPC replacing POPC. The lipid solutions were dried under vacuum for 3 h and rehydrated in MES buffer to a concentration of 0.5 mg/mL. Lipids were extruded 10 times through a 50-nm pore size polycarbonate membrane filter (GE Healthcare Life Science, Pittsburgh, PA) to form vesicles that were ~100 nm in diameter, determined by dynamic light scattering (Malvern Instruments, Worcestershire, UK).

Fusion assay

Fusion experiments were performed inside microfluidic devices. The device assembly procedure is provided in the Supporting Material. The outlet tubes of the microfluidic device were attached to a syringe pump while the inlet tubes were placed in a vial containing a loading solution. The first loading solution contained the lipid vesicles, which were

drawn into the microfluidic device to form a supported lipid bilayer (SLB) over the course of 20 min. This SLB acts as the target membrane for the virus, and the SLB can either consist of composition A (SLB A) or B (SLB B). Excess vesicles were rinsed away by flowing MES buffer through the device channels. Virions were loaded into the channels and then allowed to bind to the G_{D1a} in the bilayer. Unbound virions were rinsed away with MES buffer. Fusion was triggered by flowing in a citric acid buffer (1 mM citric acid, 150 mM NaCl) at prescribed pH values at a flow rate of 500 μL/min for 30 s (see Fig. S1 in the Supporting Material).

Hemifusion lag-time data from experiments

The R18-labeled virus was observed through total internal reflection fluorescence microscopy using an inverted microscope (Carl Zeiss, Oberkochen, Germany) and a 100× oil-immersion objective. Two lasers (561-nm and 488-nm) illuminated the labeled virus and the Oregon Green in the bilayer. When the acid reached the bilayer, the Oregon Green fluorophores quenched in the target bilayer and the R18 fluorophores in the virus dequenched upon lipid mixing. The time between these events is the lag time for hemifusion. In this work, we use the terms "fusion" and "hemifusion" interchangeably to describe the merging of two outer leaflets of the viral and target membrane. Fig. S1 shows how the fusion lag time is determined; additional details about fusion lag-time acquisition can be found elsewhere (21,23,29).

Target membrane quality and lipid diffusivity

The diffusion coefficients of R18 fluorophores in the supported lipid bilayers at various pH conditions were determined using fluorescence recovery after photobleaching (FRAP). FRAP was performed to check the bilayer quality and detect changes in membrane properties. FRAP experiments and analyses are described in the Supporting Material and in Fig. S2.

SIMULATION METHODS

Defining the spatial domain with a two-dimensional hexagonal lattice

The spatial domain of the simulation is defined as a two-dimensional plane representing the overlapped projection of the viral and target membrane, similar to the setup used by Schreiber et al. (19). To capture some three-dimensional aspects of fusion, such as the curvature of the viral membrane, we define two regions in the spatial domain: the contact area and the surrounding area. In the contact area, the viral and host membrane are located at an optimal distance from each other to allow HA trimers to mediate receptor binding and membrane fusion. In the surrounding area, the HA trimers are too far away from the target membrane to interact with the receptor. Note that due to the two-dimensional spatial system, fusion intermediate structures, such as the hemifusion stalk and membrane dimples, cannot be shown visually, but their formation can still be described kinetically by associating these structures with distinct species that occupy space within the simulation spatial domain.

The spatial domain was discretized into a lattice array as a coarse-graining strategy to reduce simulation time at the cost of losing spatial resolution. We used a hexagonal lattice, instead of a square lattice, because tightly-packed HA trimers tend to adopt a triangular arrangement (30,31). To simulate HA positions more realistically, a continuous spatial domain could be deployed using an off-lattice system. However, such a simulation method would be considerably more computationally expensive. If HA trimers must be close together to cooperatively induce fusion, then the hexagonal lattice suffices in capturing this arrangement of HA trimers.

The circumdiameter of one hexagonal unit was set at 6 nm to match the diameter of an HA trimer (7,10); this lattice element size ensures that HA trimers will not physically overlap. The total simulation space size was set at 25 × 25 grid elements (14,625 nm^2), or roughly half the surface area of a spherical virus with a diameter of 100 nm. A larger spatial domain could be used, though this may be unnecessary because fusion occurs at a smaller contact area. The contact area was approximated as a 10 × 10 lattice domain (2338 nm^2) positioned in the center of the entire simulation space. The influenza strains we are studying are generally spherical and span a range of diameters between 85 and 170 nm (32,33). To determine whether the contact area size has an impact on the values obtained for w and q, we also considered other contact area sizes. In short, w and q were not sensitive to contact area size (see the Supporting Material and Fig. S6).

Defining the simulation species

The total number of receptors, R, was set arbitrarily to 65, whereas the number of HA trimers was varied depending on the approach being used. All species were placed randomly across the entire spatial domain. The maximum number of HA trimers used in our simulation was set to 200, to be consistent with the HA density of a typical 100-nm-diameter virion that contains roughly 400 HA trimers (34). This maximum HA number density is referred to as $\rho_{HA,200}$. Note that Imai et al. (13) report the unit of HA density as a weight ratio of HA to lipid. Our $\rho_{HA,200}$ corresponds to their maximum HA density and a 3.4 HA/lipid mass ratio.

There are two types of HA trimers in our model, HA_0 and $HA_{1,2}$. Both can bind to receptor R, but only $HA_{1,2}$ can undergo conformational change to become an $HA_{1,2}$* species. An HA species can move laterally to an adjacent free grid element that has no HA in it, and a similar rule applies for

R as well. An HA and an R can overlap the same grid element because HA and R exist in two different membranes. An $HA_{1,2}$* inside the contact area is interpreted as an HA trimer that has inserted its fusion peptide into the target bilayer, and this is then treated as an immobile species. Here, fusion peptide insertion can occur without receptor binding (1,35,36), which is also consistent with several reports showing that receptor binding is not required for fusion (22,37–41). Table S2 summarizes the species involved in our simulation and their permitted locations in the simulation space.

The positions of HA trimers are important when defining a fusible unit species. A fusible unit is defined by an arrangement of HA (HA_0 or $HA_{1,2}$) and $HA_{1,2}$* species in adjacent grid elements that is characterized by w and q. An example of a $w = 3$ and $q = 1$ criterion for forming a fusible unit is shown in Fig. 1; examples of other arrangements that were tested are provided in Supporting Material and Fig. S4. Note that the actual number of conformationally changed HA trimers inside the fusible unit arrangement can exceed q and follow a distribution; however, q itself cannot follow a distribution because q represents the minimum number of conformationally changed HA trimers that are required for fusion.

An unresolved issue remains whether or not the fusible unit consists of an irreversible aggregation of HA trimers. Based on the EM picture provided by Kanaseki et al. (6), aggregated HA trimers are not apparent before or after fusion. Aggregation has been theorized mainly due to the rosette seen after the acidification of HA trimers (4). The fusible unit in our model is not an aggregated HA trimer complex, but rather it is a transient configuration in the contact area where HA trimers can pinch the target bilayer into a dimple. Once a fusible unit is identified within the contact area, it is treated as a distinct simulation species that can transition into a bent complex intermediate, which is analogous to the fusion dimple observed in EM studies of influenza membrane fusion (5,6). The bent complex can then proceed to a merged state of the outer leaflets of the two membranes, defined as a hemifusion stalk. The time when the first hemifusion stalk appears dictates the fusion lag time in both the fusion simulations and experiments. Fig. 1 shows the simulated reaction/diffusion events and Table 1 summarizes the rate parameter values used in this work (17,19,42,43).

Defining the reaction rate parameters

The hopping rate of HA or *R* from one grid element to an adjacent element is defined as $k_{diff,HA}$ and $k_{diff,R}$, respectively. These parameters were calculated from their corresponding diffusion coefficients as described in the Supporting Material. The binding and unbinding rates between an HA trimer and receptor, defined as k_{bind} and k_{unbind}, respectively, were adopted from the work of Schreiber et al. (19). Note that Imai et al. (13) used glycoprotein on red blood cells as the viral receptor, whereas we used G_{D1A} glycolipid instead. Hence, the $k_{diff,R}$ value for glycoprotein (i.e., 74 s^{-1}) was used to simulate the data of Imai et al., whereas the $k_{diff,R}$ value for G_{D1A} (capped at 2000 s^{-1}) was used when simulating our own data.

The activation rate, k_{act}, of an HA trimer as a function of pH has been determined experimentally by Krumbiegel et al. (43) for the X31 virus (H3N2) that we are using. They report a k_{act} value of 5.78 s^{-1} for pH conditions that are <4.9. Because Imai et al (13) performed experiments at a higher pH value of 5.2 and with a different HA serotype (H1), a different k_{act} value had to be used to simulate their data. But, to our knowledge, k_{act} is unknown for the H1 serotype of HA trimer, therefore as a starting point, we used the k_{act} value (0.067 s^{-1}) for the H3 serotype at a pH value of 5.2 that was found by Krumbiegel et al. (43). We then tested another arbitrary k_{act} value of 0.010 s^{-1} to see how this affects our conclusion for w and q. Results for these tests are provided in the Supporting Material and in Fig. S7; in short, our conclusions on w and q did not depend on k_{act} within the tested range.

A lumped rate parameter that describes how fast a fusible unit can bend the target membrane is defined as k_{bend}. Parameter k_{bend} depends on both the HA trimer's ability to bend the membrane as well as the properties of the target membrane that dictate its ability to bend. The value for k_{bend} is unknown and k_{bend} is an important fitting parameter in our model. An approximate value for k_{bend}, which we denote as $k_{bend,approx}$, is found by adjusting k_{bend} until the simulated distribution is not statistically different from the actual distribution according to a Kolmogorov-Smirnov (KS) test, as described below. When a more precise value of k_{bend} is necessary to make conclusions about membrane bending rates, which is the case when studying k_{bend} as a function of pH or membrane properties, k_{bend} is refined using a bootstrap method (44). This refinement method is described in the Supporting Material. The k_{bend} values reported later in Figs. 5 and 6 have been refined.

The frequency rate at which a highly bent target membrane transitions into a hemifusion stalk, k_{merge}, is expected to be similar in magnitude to that for vesicle-vesicle fusion. Lentz and Lee (45) provided a comprehensive review on the similarities between PEG-induced and HA-induced fusion. The half-life for PEG-induced fusion is ~10 s (45,46), which, if fitted to the equation $k_{merge} = -\ln(1/2)/t_{1/2}$, gives an associated rate constant of 0.07 s^{-1}. To find a value for k_{merge} that is most representative of an influenza virus fusing with a host membrane, we look to existing fusion data in the pH range where HA conformational change is not limited by proton availability. Floyd et al. (21) showed that at pH 3, the fusion lag-time distribution reflects a single rate-limiting step with a rate constant of 0.1 s^{-1}. If the rate-limiting step is the merging of the membrane at this low pH, then the rate constant value of 0.1 s^{-1} is in good agreement with that estimated from PEG-induced vesicle fusion studies. We therefore assigned k_{merge} to be 0.1 s^{-1} in our simulation model.

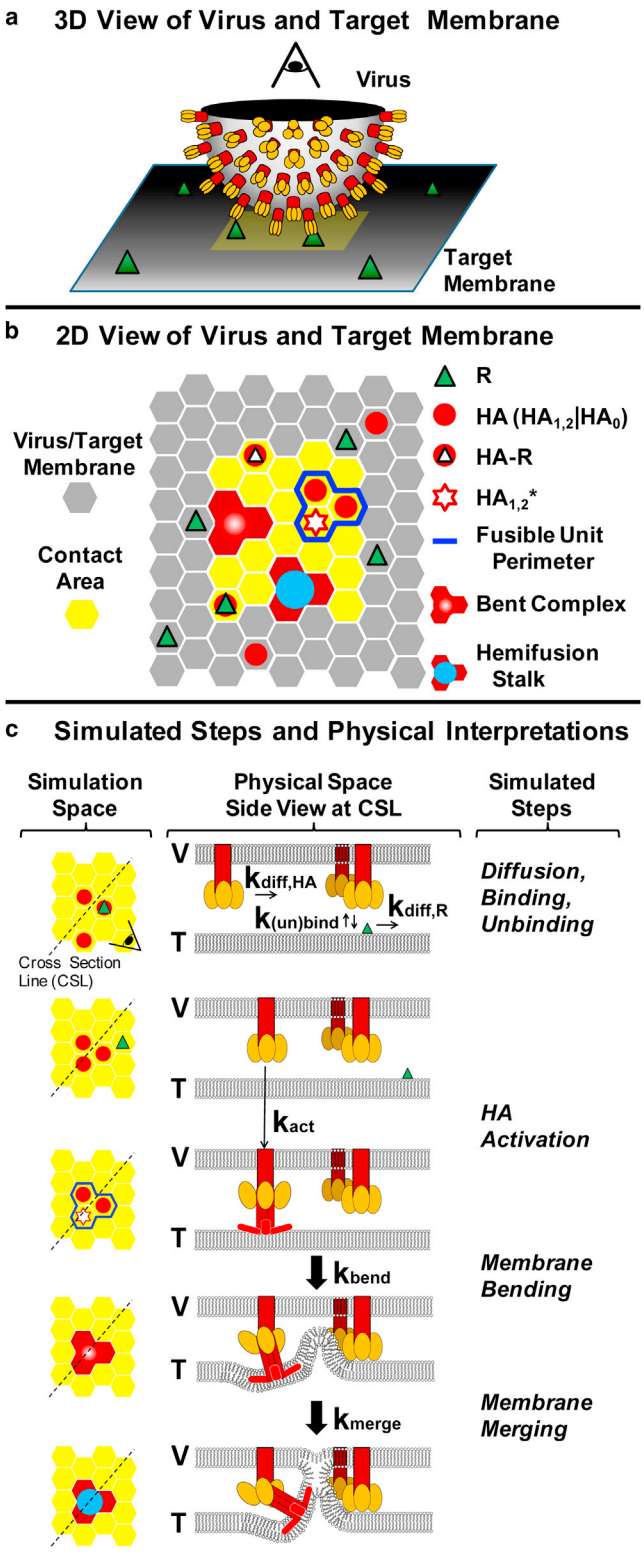

FIGURE 1 Virus-cell interaction represented in the simulation space. (*a*) A close-up, three-dimensional view of half of the virus bound to the host membrane. (*b*) Two-dimensional representation of the three-dimensional picture. The simulation space represents the viral membrane overlapping the target membrane. The HA and R species move within a hexagonal lattice domain. Any interaction between the virus and host membrane occurs within the contact area (*yellow*). An example of using a $w = 3$, $q = 1$ criterion for forming a fusible unit is outlined (*blue perimeter*). (*c*) Catalog of simulated events in the fusion model. The simulation species are shown on the left-hand side as a top-down view; the corresponding physical interpretations of the species are shown in the middle through cross-sectional side views. The viral and target membranes are labeled *V* and *T*, respectively. (*Yellow ovals*) HA_1 binding domain; (*red objects*) HA_2 fusion domain of an $HA_{1,2}$ trimer. (*Brighter red*) Portions of the HA_2 domain representing the hydrophobic fusion peptides that inserts into the target membrane. To see this figure in color, go online.

Technique for simulating hemifusion lag time

Our simulation uses the stochastic simulation algorithm developed by Gillespie (47) to predict the lag time for a virus hemifusion event. Any changes to a simulation species or its position are treated as a reaction event. The probability of a reaction event occurring within a small time increment, $[t, t + dt]$, is defined as a "propensity". The propensity of a reaction event is calculated from both the rate parameters and the number of species involved for each reaction event. At a simulated time of $t = 0$, the system is considered to be acidified and fusogenic HA trimers are allowed to change conformation and participate in forming a hemifusion stalk. Using a random number generator and an iterative loop, all reaction events can be simulated based on their propensities. The formation of the first hemifusion stalk species dictates the fusion lag time and ends the simulation. Simulations are repeated 1000 times to collect a distribution of lag times. More details on the simulation algorithm are provided in the Supporting Material.

Matching simulated and actual fusion lag-time distributions

To determine if the simulated lag-time distribution is an acceptable fit for the experimental data, the two-population KS test (48,49) was used. The null hypothesis for the KS test is that two distributions are statistically the same. If the KS statistic (D_{test}), defined as the greatest vertical distance between two normalized cumulative lag-time distributions, is greater than the critical KS statistic (D_{crit}) for a 5% significance level, then the null hypothesis is rejected. The critical KS statistic is calculated using the equation below, where $c(\alpha) = 1.36$ for the 5% significance level, n_{exp} = number of data points from experiment, and n_{sim} = number of data points from simulation:

$$D_{\text{crit}} = c(\alpha)\sqrt{\frac{n_{\text{sim}} + n_{\text{exp}}}{n_{\text{sim}} n_{\text{exp}}}}.$$

- If $D_{\text{test}} \geq D_{\text{crit}}$, simulation results are rejected.
- If $D_{\text{test}} < D_{\text{crit}}$, simulation results are accepted.

The criteria for accepting a simulation result is that D_{test} must be less than D_{crit}, which means the simulated distribution is not statistically different from the experimental

TABLE 1 List of simulated reaction events and their associated symbols and values

Reaction event	Rate symbol	Rate value (s^{-1})
Diffusion of HA and R		
$HA(\mathbf{r}_1) \rightarrow HA(\mathbf{r}_2)$	$k_{diff,HA}$	740 (17)
$R(\mathbf{r}_1) \rightarrow R(\mathbf{r}_2)$	$k_{diff,R}$ (Glycoprotein)	[74] (19,42)
	$k_{diff,R}$ (G_{D1a})	2000[a]
Actions of HA and R		
HA + R → HA-R	k_{bind}	0.20 (19)
HA-R → HA + R	k_{unbind}	0.15 (19)
$HA_{1,2} \rightarrow HA_{1,2}$*	k_{act} (pH = 5.2)	[0.067][b]
	k_{act} (pH < 4.9)	5.78 (43)
Membrane events		
[Fusible unit] → [bent complex]	k_{bend}	Fitted parameter
[Bent complex] → [hemifusion stalk]	k_{merge}	0.10

HA refers to either HA_0 or $HA_{1,2}$. The bracketed rate parameter values were used only when matching the data of Imai et al. (13). The numbers in parentheses are the references from which these values were taken.
[a]Capped value. See text and the Supporting Material for more details.
[b]k_{act} values for the H1 serotype of HA in the virosomes of Imai et al. (13) are unknown. Values of 0.01 s^{-1} and 0.067 s^{-1} were tested. More details are provided in the Supporting Material.

distribution within the 95% confidence interval. Values for D_{test} and D_{crit} are provided in the legends of the figures that show the lag-time distributions (Figs. 2, 5, and 6).

Determining rate-limiting steps using sensitivity analysis

To determine the rate-limiting steps (RLSs) for fusion, the common strategy of comparing the magnitude of rate parameters could not be used because this neglects the fact that multiple HA trimers can act in parallel to induce fusion. Another way to determine the RLSs is to make use of the fact that the fusion lag-time output will be most sensitive to the RLSs; hence, a sensitivity analysis was performed for each rate parameter. To perform the sensitivity analysis, the rate parameter being evaluated was adjusted by 10 and 20% from the current value while other parameters were fixed, and simulations were run to extract the new, altered lag-time distributions. A sensitivity index, S_a, is calculated for each rate parameter using the formula (25,50)

$$S_a = \frac{\partial Y}{\partial p} = \frac{|Y_{alt} - Y_{ref}|}{|p_{alt} - p_{ref}|},$$

where Y_{alt} is the mean lag time obtained at the altered parameter value p_{alt}, and Y_{ref} is the mean lag time obtained at the original value of the parameter p_{ref}. The RLSs are associated with the rate parameters with the highest, relative sensitivity index values.

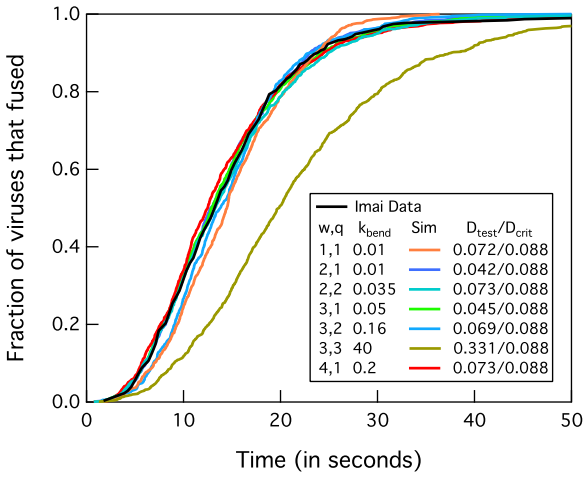

FIGURE 2 Determining possible solutions for w, q, and k_{bend} using the Constant FB approach on the fusion data of Imai et al. (13) at $\rho_{HA,200}$ and using rate values in Table 1 for pH 5.2. The ratio D_{test}/D_{crit} is used to determine if simulations match with the data of Imai et al. If D_{test}/D_{crit} is <1, simulations are accepted. An example of an invalid solution is shown when $w = 3$ and $q = 3$ (*olive green line*), as noted by D_{test}/D_{crit} being >1. To see this figure in color, go online.

RESULTS

Overview of the strategy for determining *w* and *q*

The unknown parameters in our model are w, q, and k_{bend}. We begin by using the Constant FB approach to find multiple valid combinations of w, q, and k_{bend} that allow the simulated lag-time distributions to match that of Imai et al. (13) when the $HA_{1,2}$ density is $\rho_{HA,200}$ (Fig. 2, *black line*). The rate parameters that were used for this step are listed in Table 1 for the experimental system of Imai et al., which involves virosomes with HA trimer (H1 serotype) binding to glycoprotein receptors and fusing with a cell membrane at a pH of 5.2. We then use the Variable F and FB approach to find a unique solution for w, q, and k_{bend} by matching the simulated trends in fusion rates versus HA densities with the trends of Imai et al. (13). After a unique solution of w, q, and k_{bend} is determined, we retain the w and q values and perform a model validation procedure to see if the model can predict the fusion kinetics of the H3N2 (X31) influenza virus.

The model is validated if simulated lag-time distributions match with those from X31 fusion experiments performed at different pH conditions and membrane compositions. Because the HA densities were not varied, this process is categorized under the Constant FB approach. The rate parameters that were used are listed in Table 1 for our experimental system, which involves the H3N2 virus binding to G_{D1A} receptors and fusing with a supported lipid bilayer at a pH between 3 and 4.5. We assumed w and q are constant across the H3 and H1 serotypes of HA trimers and for the experimental conditions used here. Parameter k_{bend} was left as the sole fitting parameter while all other parameters were held constant. If the simulations cannot match the lag-time distributions found from fusion experiments

through the adjustment of k_{bend}, then the model assumptions are invalid and need to be revised. If simulations can match with experiments, then the model assumptions are validated and the resulting solution for w and q is accepted. The above simulation strategy is summarized in a flow chart provided in Fig. S5.

Finding potential solutions for w, q, k_{bend} using Constant FB

The Constant FB approach was used to simulated lag-time distribution from Imai et al. (13) when the $HA_{1,2}$ density is $\rho_{HA,200}$ and the pH is 5.2. The rate parameters (besides k_{bend}) used are shown in Table 1 for the experimental system of Imai et al. (13), which were held constant. Fig. 2 shows the matched cumulative fusion lag-time distributions for many combinations of w, q, and k_{bend}. Note that this also shows that the Constant FB approach cannot be used alone to find a unique solution for w and q. Variable F and FB approaches are needed to reduce the number of solutions.

Eliminating w, q, k_{bend} solutions using Variable F

For each possible solution of w, q, and k_{bend} found above, simulations were run to mimic the Variable F approach of Imai et al. (13) to see which set of values could recapitulate results from their experimental data set. In the simulation, the number of $HA_{1,2}$ trimers was incrementally decreased from 200 to 10 while the number of HA_0 trimers was incrementally added so that the total number of HA trimers in the simulation space remained constant at 200. The cumulative lag-time distributions for each concentration of $HA_{1,2}$ were then plotted and the maximum slope, V_{max}, was determined for each distribution for each $HA_{1,2}$ density. The slope value of Imai et al. (13) for a plot of log V_{max} versus log [$HA_{1,2}$] from the Variable F approach is 0.85 (95% confidence interval (CI), between 0.63 and 1.08). Simulation yields a slope value within the 95% CI from Imai et al. (13) when q is 1 (Figs. 3 *a* and 4) and w is 2 or 3. The slope value increased with higher q values (Figs. 3 *a* and 4), and therefore values of $q > 3$ did not need to be tested because this would cause simulation results to diverge further from the results of Imai et al.

Eliminating w, q, k_{bend} solutions using Variable FB

For each possible solution of w, q, and k_{bend}, simulations were also run to mimic the Variable FB approach (13). Here, the number of $HA_{1,2}$ trimers was incrementally decreased from 200 to 10 and no HA_0 trimers were present. The slope value of Imai et al. from the plot of log V_{max} versus log [$HA_{1,2}$] for the Variable FB approach is 2.2 (95% CI between 1.55 and 2.79). The simulation slope value falls within the 95% CI of Imai et al. (13) when w is 2 or 3 and q is 1 (Figs. 3 *b* and 4). The slope value increased with

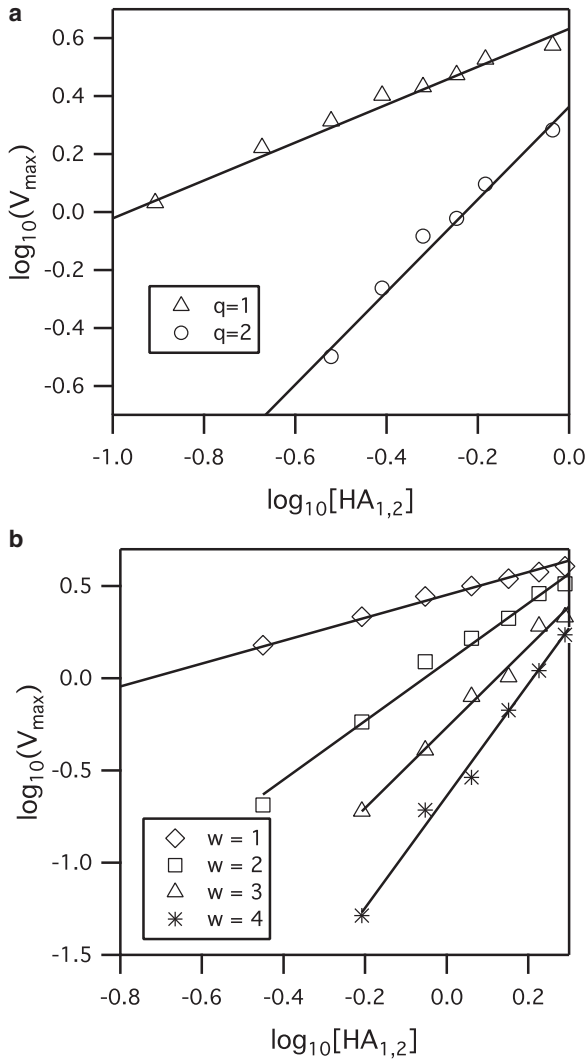

FIGURE 3 Sample simulation log-log plot of V_{max} versus $HA_{1,2}$ density for (*a*) Variable F approach for the condition that $w = 3$ while q is varied. The slopes of the best-fit lines are 0.65 and 1.6 for $q = 1$ and 2, respectively. (*b*) Variable FB approach for $q = 1$ while w is varied. The slopes of the best-fit lines are 0.62, 1.59, 2.19, and 3.03 for w values of 1, 2, 3, and 4, respectively. The r^2 values for all regression lines are at least 0.99. The unit of HA density, [$HA_{1,2}$], has been converted to its corresponding mass ratio of HA to lipid to be consistent with the results of Imai et al. (13).

higher values of w; therefore, values of $w > 4$ did not need to be tested as this would cause simulation results to diverge further from the results of Imai et al.

The combinations of w and q that agree with both Variable F and FB results in Imai et al. (13) are either $w = 3$ and $q = 1$, or $w = 2$ and $q = 1$. Other combinations of w and q failed to match at least one data set of Imai et al. (13). We concluded that w is more likely to be 3 instead of 2 because for the Variable FB results, the 95% CI for simulation slope values falls completely inside that of the 95% CI from Imai et al. (13) only when $w = 3$. But regardless of whether the value of w is 2 or 3, any value of $w > 1$ suggests HA trimers act cooperatively to induce fusion.

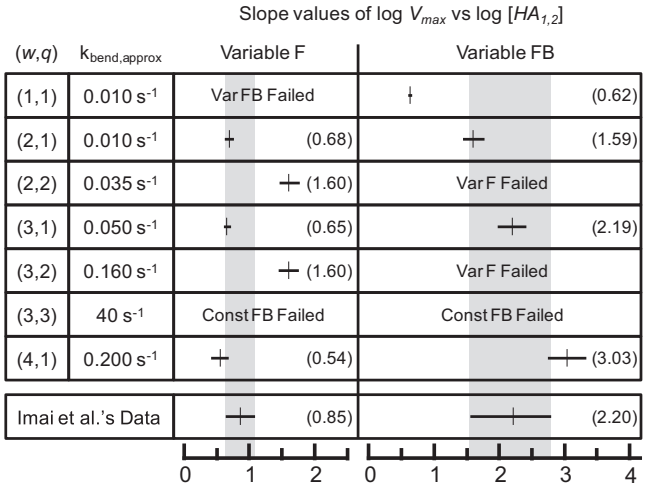

FIGURE 4 Slope values of log V_{max} versus log [$HA_{1,2}$] for various combinations of w and q values. Some simulations were unnecessary due to the inability to yield results that are consistent with the fusion data of Imai et al. (13). (*Shaded bar*) 95% confidence interval of the data of Imai et al. (13). The numerical values of the slopes are provided in parentheses.

Validating simulation model using Constant FB at varying pH conditions

Fusion experiments were performed with the X31 (H3N2) virus and SLB A at several pH conditions, and corresponding simulations were run to validate the model against this data. By adjusting only k_{bend}, while holding w and q constant and using the appropriate rate parameter values in Table 1 for our experimental system, the simulation model was able to replicate the kinetic data (Fig. 5 *a*) from fusion experiments. Note that $k_{diff,R}$ is now 2000 s^{-1} because we used G_{D1A} as the receptor, and k_{act} is 5.78 s^{-1} because experiments were done at a pH < 4.9. The good agreement between simulations and experiments validates our model and assumption that w and q do not change over the range of pH values tested and across the HA protein serotypes of H1 and H3.

A closer look at the simulation results shows that the k_{bend} values for pH 4.0 and 4.5 are considerably smaller than those for pH 3.5 and 3.0, but k_{bend} is still a nonzero number (Fig. 5 *b*). Recall that k_{bend} represents both the HA trimer's ability to bend the target membrane and the deformability of the membrane itself. One interpretation of a smaller k_{bend} value is that the HA trimers are having more difficulty bending the target membrane. Another possible explanation is that the target membrane itself is harder to bend due to changes in membrane properties, as suggested by the decreasing diffusion coefficient of R18 membrane fluorophores in the SLB at higher pH conditions (Fig. 5 *b*). We note that the diffusion coefficient itself is not a measure of membrane flexibility but is merely used here as an indicator to show that the target membrane has changed in some way. This change could be embodied as a change in lipid packing due to different pH conditions or ionic strengths (51,52).

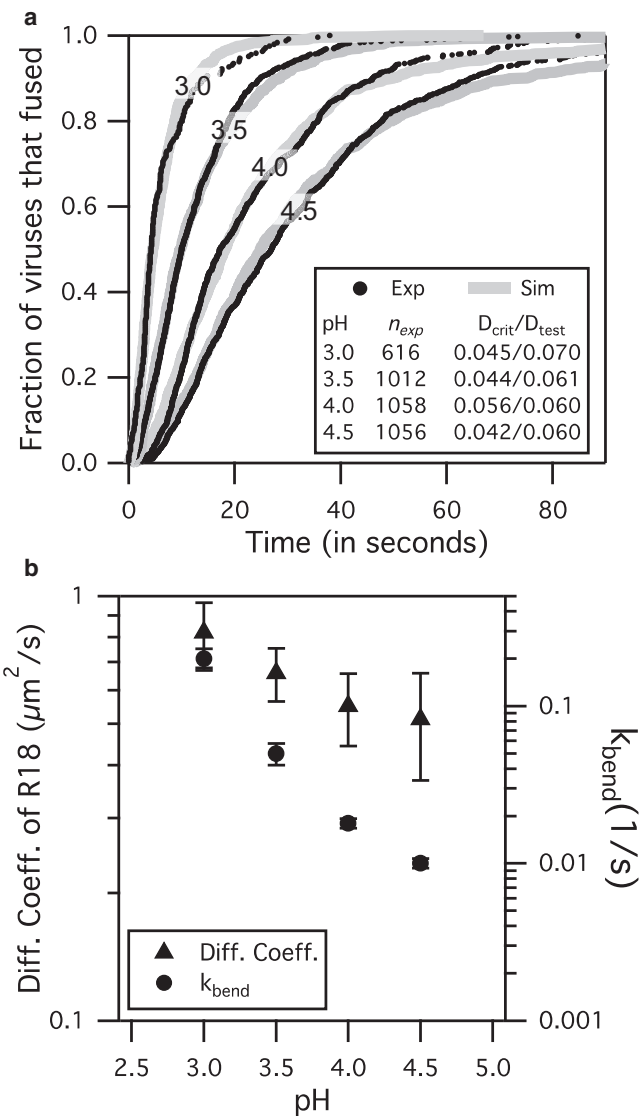

FIGURE 5 X31 fusion results at various pH conditions for SLB A at $\rho_{HA,200}$. (*a*) Simulations are able to fit experimental data by adjusting only k_{bend} while keeping $w = 3$ and $q = 1$. (*b*, *right axis* and *circles*) The mean k_{bend} values for pH 3.0, 3.5, 4.0, and 4.5 are 0.2, 0.05, 0.018, and 0.01 s^{-1}, respectively, with standard deviation shown in error bars. (*b*, *left axis* and *triangles*) The mean R18 diffusivity values for pH 3.0, 3.5, 4.0, and 4.5 are 0.82, 0.66, 0.55, and 0.51 μm^2/s, respectively, with standard deviation shown in error bars. Mobile fractions of R18 were close to 1 for all cases. Both R18 diffusivity and k_{bend} decrease with increasing pH over this range.

Validating the simulation model using Constant FB at two target membrane compositions

To further confirm that fusion is affected by target membrane properties, we changed the composition of the target membrane by replacing POPC with LPC lipid (i.e., used composition SLB B). LPC lipid has been shown to impede fusion (27) by hindering the bending of membranes. Indeed, fusion experiments at pH 4.0 show that viruses fused much more slowly with SLB B than with SLB A (Fig. 6). In

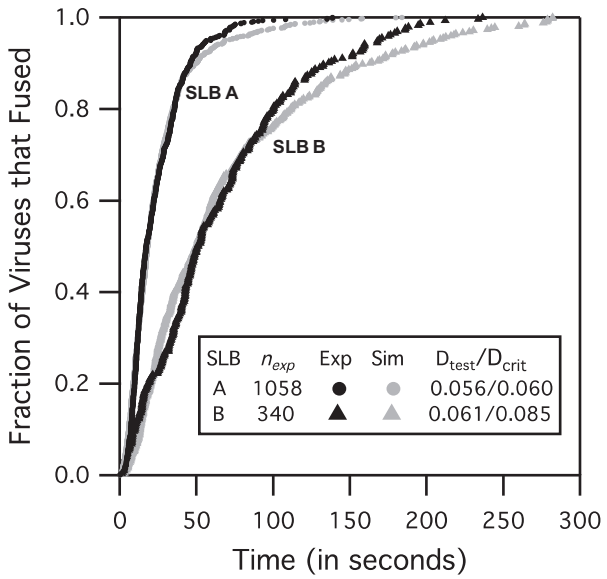

FIGURE 6 X31 virus fusion results at pH 4.0 using SLB A and SLB B. Simulations were able to match experimental data for two different target membranes membrane compositions by adjusting k_{bend} only. The values of k_{bend} from the fits are 0.018 ($\pm$0.001) s^{-1} for SLB A and 0.0035 ($\pm$0.0002) s^{-1} for SLB B.

addition, simulations were able to match both SLB A and SLB B fusion lag-time data by adjusting only k_{bend}. Parameters w and q did not have to be altered to fit the data, suggesting that they are not sensitive to changes in membrane properties between SLB A and SLB B. The strong dependence of k_{bend} on target membrane properties agrees well with the finding of Chernomordik et al. (28) that fusion is sensitive to target membrane properties at a step after the HA activation, but before the merging of the membrane.

Note that for the same bilayer composition, higher lipid mobility is indicative of a more fluid membrane, which should be easier to bend. However, comparisons of membrane mobility across different SLB compositions to rank membrane flexibility are not appropriate because other factors such as lipid shape, bilayer elasticity, and bilayer thickness can also affect the membrane flexibility. We emphasize that the work here focuses on fluidlike membrane compositions; we have not simulated or examined other membrane types, e.g., raftlike membranes, which could cause the assumptions made earlier about the model to become invalid. Hence, we restrict our model results to apply only under such experimental conditions and fluid target membrane compositions as those used here and in the work of Imai et al. (13).

Sensitivity analysis result

A sensitivity analysis was performed on the simulation model to determine how sensitive the lag-time distribution is to slight perturbations to the rate parameters. In this case, the rate parameters that lead to the greatest change in fusion lag-time output when perturbed is associated with the rate-limiting steps of fusion, as described above in Simulation Methods. Sensitivity analysis was done for X31 fusion simulations at pH 3 and 4.5 conditions for when SLB A is the target membrane. The sensitivity index values for each of the simulation rate parameters (Fig. 7) were calculated according to the method described in Simulation Methods.

At pH 4.5, both k_{bend} and k_{merge} are sensitive parameters relative to the other parameters, suggesting that two steps, membrane bending and merging, are dominating all the others and are rate-limiting. However, at pH 3.0, k_{merge} is the most sensitive parameter relative to other parameters, suggesting that one step, i.e., membrane bending, is rate-limiting. To confirm these results, we compared them to the number of rate-limiting steps predicted by the γ-distribution fitting strategy (21,53). The γ-distribution fits resolve parameters N and k, which represent the number of significant rate-limiting steps and the observed rate constant for each step, respectively. At pH 4.5, a γ-fit yields $N = 2.04 \pm 0.02$ and $k = 0.07 \pm 0.01$ s^{-1}, agreeing with our

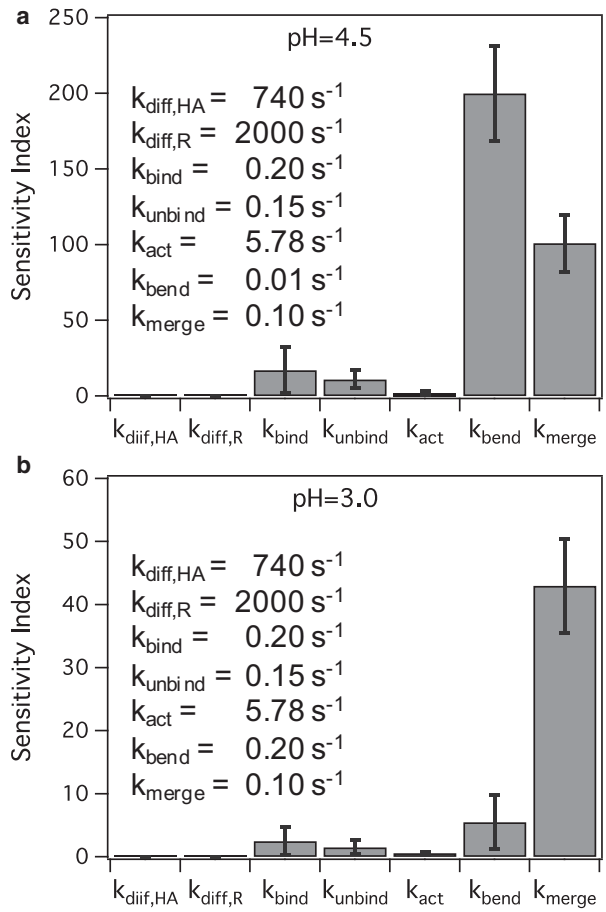

FIGURE 7 Sensitivity index values for rate parameters at (*a*) pH 4.5, where both k_{bend} and k_{merge} have large sensitivity index values relative to other parameters and (*b*) pH 3.0, where k_{merge} is the most sensitive parameter. The parameter values are provided in the legend of each plot.

sensitivity analysis that shows two rate-limiting steps. At pH 3.0, a γ-distribution fit yields $N = 1.12 \pm 0.06$ and $k = 0.15 \times 0.01\ s^{-1}$, agreeing with the sensitivity analysis showing one rate-limiting step. Note that when N is close to 1, the γ-fit k of 0.15 s^{-1} is similar in value to that for k_{merge} of 0.1 s^{-1}. Recall that k_{merge} was estimated from the γ-fit data of Floyd et al. (21) at pH 3, in which $N = 1$ and $k = 0.1\ s^{-1}$.

The remaining rate parameters, besides those of k_{merge} and k_{bend}, appear to be insensitive parameters that do not affect fusion lag times much for the X31 virus at pH conditions 4.5 or lower, as shown in Fig. 7. There are several explanations for these observations. The tight-packing of HA trimers and immobilization of HA trimers at the contact area due to receptor binding and membrane insertion may render HA diffusion negligible at the contact area. Fusion lag times are weakly sensitive to receptor binding and unbinding because HA trimers were allowed to participate in fusion regardless of receptor binding, to be consistent with prior work showing that binding is not necessary for fusion (22,37–41). Lastly, the HA activation rate does not contribute significantly to the fusion lag time because we are studying X31 fusion kinetics at a pH value <4.9 where the conformational change is fast (43) and is not expected to be rate-limiting.

DISCUSSION

Due to some similarities between ours and the simulation model of Schreiber et al. (19), we provide a more detailed comparison between the two. The main similarities are that both used the stochastic simulation algorithm (47) to simulate fusion kinetics and the spatial domain was setup up similarly. The differences are many:

1. Our spatial domain distinguishes between a contact area and the surrounding area whereas the spatial domain of Schreiber et al. represents only the contact area.
2. Their model considers that all HA trimers have undergone conformational change a $t = 0$, whereas we simulate the conformational change through rate parameter k_{act}.
3. Contrary to the model of Schreiber et al. (19), we do not assume $w = q$ and we allowed fusion to occur without receptor binding (22,37–41).
4. The model of Schreiber et al. (19) does not simulate the rate of membrane bending. Our model simulates membrane bending by including the transition rate of a fusible unit to a bent complex, granting us the ability to capture the dependence of fusion rate on target membrane properties (26–28).

According to our results, the minimum number of HA trimers required for fusion is three, but at least one HA trimer has to undergo conformational change ($w = 3, q = 1$). These results have not yet been tested against HA serotypes beyond H1 and H3, or for other experimental systems that do not involve virions or virosomes fusing to a fluid target membrane. Additionally, the results are valid only under the assumptions made when building the model. Whether or not this w and q pair applies for the other systems would be an interesting future study.

The practicality of q being 1 is reasonable when one considers the energy required to form a hemifusion stalk (54–57). The energy released by the conformational change of an HA trimer has been estimated to be ~125 k_BT (58), which is more than enough energy to form a hemifusion stalk that requires ~40 k_BT of energy (57).

The roles of the neighboring HA trimers that do not change conformation during membrane fusion, referred to as HA_{adj}, are unknown. We hypothesize that HA_{adj} trimers act as support structures that the conformationally changed $HA_{1,2}^{*}$ trimer exploits to bend the target membrane into a sharp dimple that promotes fusion, as depicted in Fig. 1. To confirm this hypothesis, one possible experiment is to make virosomes containing inactive and active HA trimers, and observe them fusing to a target at various stages through electron microscopy. These inactive HA proteins could be one of the following:

- Uncleaved HA_0 trimers; or
- Mutated HA trimers with the fusion peptides removed; or
- HA trimers that are deactivated with antifusogenic antibodies.

A visual confirmation that a fusion dimple exists between active and inactive HA trimers would support the idea that adjacent, unchanged HA trimers could act passively to induce fusion.

To postulate why different approaches result in different conclusions about the HA-induced fusion mechanism, we summarize the insight provided by each approach:

- Variable F: Fusion experiments at varying number of fusogenic HA trimers at a constant total HA trimer density yield information about the level of cooperativity between only conformationally changed HA trimers.
- Variable FB: Fusion experiments at varying total densities of fusogenic HA trimers reveal the number of HA trimers in a fusion complex.
- Constant FB: Fitting fusion lag-time distributions, obtained at a single HA density, to statistical distributions yields quantitative information about the sequential and parallel steps leading to fusion.

The information obtained from all three approaches must be processed together to resolve the fusion mechanism from kinetic data.

CONCLUSION

The simulation model presented here demonstrates the importance of considering the differences between the three

approaches for studying membrane fusion kinetics. The mechanistic insight this model provides is that some fraction of HA trimers could potentially act passively to assist in membrane fusion, which would explain why some experiments show that HAs act cooperatively to induce fusion whereas others do not. This simulation model is the first that we know of to explicitly capture the role of the host membrane into the model through the inclusion of rate parameter k_{bend}. Although we chose to focus on the influenza virus because of the plethora of data available to validate the model, the simulation and modeling approach is general enough that it could be extended to study other viruses. Whether the model is able to accurately recapitulate the fusion behaviors of other viruses will be an interesting future study.

SUPPORTING MATERIAL

Two tables, seven figures supplemental information and References (59–62) are available at http://www.biophysj.org/biophysj/supplemental/S0006-3495(14)00078-2.

P.C. thanks Intel Corporation for provision of computing support. All authors thank Dr. Radhendushka Srivastava for helpful discussions on statistical analysis, and Professor Manfred Lindau for his insightful comments.

D.W.L. is a recipient of a National Science Foundation GK-12 Fellowship in Biomedical Engineering. V.T. was funded by the Semiconductor Research Corporation, contract No. 2012-VJ-2272. A portion of this work was funded by the National Science Foundation grant CBET-126701 to S.D.

REFERENCES

1. Doms, R. W., A. Helenius, and J. White. 1985. Membrane fusion activity of the influenza virus hemagglutinin. The low pH-induced conformational change. *J. Biol. Chem.* 260:2973–2981.
2. Skehel, J. J., and D. C. Wiley. 2000. Receptor binding and membrane fusion in virus entry: the influenza hemagglutinin. *Annu. Rev. Biochem.* 69:531–569.
3. Bentz, J. 2000. Minimal aggregate size and minimal fusion unit for the first fusion pore of influenza hemagglutinin-mediated membrane fusion. *Biophys. J.* 78:227–245.
4. Doms, R. W., and A. Helenius. 1986. Quaternary structure of influenza virus hemagglutinin after acid treatment. *J. Virol.* 60:833–839.
5. Lee, K. K. 2010. Architecture of a nascent viral fusion pore. *EMBO J.* 29:1299–1311.
6. Kanaseki, T., K. Kawasaki, …, S. Ohnishi. 1997. Structural features of membrane fusion between influenza virus and liposome as revealed by quick-freezing electron microscopy. *J. Cell Biol.* 137:1041–1056.
7. Böttcher, C., K. Ludwig, …, H. Stark. 1999. Structure of influenza hemagglutinin at neutral and at fusogenic pH by electron cryo-microscopy. *FEBS Lett.* 463:255–259.
8. Bullough, P. A., F. M. Hughson, …, D. C. Wiley. 1994. Structure of influenza hemagglutinin at the pH of membrane fusion. *Nature.* 371:37–43.
9. Wiley, D. C., and J. J. Skehel. 1987. The structure and function of the hemagglutinin membrane glycoprotein of influenza virus. *Annu. Rev. Biochem.* 56:365–394.
10. Wilson, I. A., J. J. Skehel, and D. C. Wiley. 1981. Structure of the hemagglutinin membrane glycoprotein of influenza virus at 3 Å resolution. *Nature.* 289:366–373.
11. Struck, D. K., D. Hoekstra, and R. E. Pagano. 1981. Use of resonance energy transfer to monitor membrane fusion. *Biochemistry.* 20:4093–4099.
12. Otterstrom, J., and A. M. van Oijen. 2013. Visualization of membrane fusion, one particle at a time. *Biochemistry.* 52:1654–1668.
13. Imai, M., T. Mizuno, and K. Kawasaki. 2006. Membrane fusion by single influenza hemagglutinin trimers. Kinetic evidence from image analysis of hemagglutinin-reconstituted vesicles. *J. Biol. Chem.* 281:12729–12735.
14. Bundo-Morita, K., S. Gibson, and J. Lenard. 1987. Estimation by radiation inactivation of the size of functional units governing Sendai and influenza virus fusion. *Biochemistry.* 26:6223–6227.
15. Gibson, S., C. Y. Jung, …, J. Lenard. 1986. Radiation inactivation analysis of influenza virus reveals different target sizes for fusion, leakage, and neuraminidase activities. *Biochemistry.* 25:6264–6268.
16. Günther-Ausborn, S., P. Schoen, …, T. Stegmann. 2000. Role of hemagglutinin surface density in the initial stages of influenza virus fusion: lack of evidence for cooperativity. *J. Virol.* 74:2714–2720.
17. Danieli, T., S. L. Pelletier, …, J. M. White. 1996. Membrane fusion mediated by the influenza virus hemagglutinin requires the concerted action of at least three hemagglutinin trimers. *J. Cell Biol.* 133: 559–569.
18. Ellens, H., J. Bentz, …, J. M. White. 1990. Fusion of influenza hemagglutinin-expressing fibroblasts with glycophorin-bearing liposomes: role of hemagglutinin surface density. *Biochemistry.* 29:9697–9707.
19. Schreiber, S., K. Ludwig, …, H. G. Holzhütter. 2001. Stochastic simulation of hemagglutinin-mediated fusion pore formation. *Biophys. J.* 81:1360–1372.
20. Blumenthal, R., D. P. Sarkar, …, S. J. Morris. 1996. Dilation of the influenza hemagglutinin fusion pore revealed by the kinetics of individual cell-cell fusion events. *J. Cell Biol.* 135:63–71.
21. Floyd, D. L., J. R. Ragains, …, A. M. van Oijen. 2008. Single-particle kinetics of influenza virus membrane fusion. *Proc. Natl. Acad. Sci. USA.* 105:15382–15387.
22. Stegmann, T., J. M. White, and A. Helenius. 1990. Intermediates in influenza induced membrane fusion. *EMBO J.* 9:4231–4241.
23. Costello, D. A., D. W. Lee, …, S. Daniel. 2012. Influenza virus-membrane fusion triggered by proton uncaging for single particle studies of fusion kinetics. *Anal. Chem.* 84:8480–8489.
24. Ivanovic, T., J. L. Choi, …, S. C. Harrison. 2013. Influenza-virus membrane fusion by cooperative fold-back of stochastically induced hemagglutinin intermediates. *eLife.* 2:e00333.
25. Dobay, M. P., A. Dobay, …, E. Mendoza. 2011. How many trimers? Modeling influenza virus fusion yields a minimum aggregate size of six trimers, three of which are fusogenic. *Mol. Biosyst.* 7:2741–2749.
26. Razinkov, V. I., G. B. Melikyan, …, F. S. Cohen. 1998. Effects of spontaneous bilayer curvature on influenza virus-mediated fusion pores. *J. Gen. Physiol.* 112:409–422.
27. Chernomordik, L., A. Chanturiya, …, J. Zimmerberg. 1995. The hemifusion intermediate and its conversion to complete fusion: regulation by membrane composition. *Biophys. J.* 69:922–929.
28. Chernomordik, L. V., E. Leikina, …, J. Zimmerberg. 1997. An early stage of membrane fusion mediated by the low pH conformation of influenza hemagglutinin depends upon membrane lipids. *J. Cell Biol.* 136:81–93.
29. Wessels, L., M. W. Elting, …, K. Weninger. 2007. Rapid membrane fusion of individual virus particles with supported lipid bilayers. *Biophys. J.* 93:526–538.
30. Wrigley, N. G. 1979. Electron microscopy of influenza virus. *Br. Med. Bull.* 35:35–38.
31. Hess, S. T., M. Kumar, …, J. Zimmerberg. 2005. Quantitative electron microscopy and fluorescence spectroscopy of the membrane distribution of influenza hemagglutinin. *J. Cell Biol.* 169:965–976.
32. Vijayakrishnan, S., C. Loney, …, D. Bhella. 2013. Cryotomography of budding influenza A virus reveals filaments with diverse morphologies

that mostly do not bear a genome at their distal end. *PLoS Pathog.* 9:e1003413.

33. Harris, A., G. Cardone, …, A. C. Steven. 2006. Influenza virus pleiomorphy characterized by cryoelectron tomography. *Proc. Natl. Acad. Sci. USA.* 103:19123–19127.
34. Ruigrok, R. W. H., P. J. Andree, …, J. E. Mellema. 1984. Characterization of three highly purified influenza virus strains by electron microscopy. *J. Gen. Virol.* 65:799–802.
35. Skehel, J. J., P. M. Bayley, …, D. C. Wiley. 1982. Changes in the conformation of influenza virus hemagglutinin at the pH optimum of virus-mediated membrane fusion. *Proc. Natl. Acad. Sci. USA.* 79:968–972.
36. Gething, M. J., R. W. Doms, …, J. White. 1986. Studies on the mechanism of membrane fusion: site-specific mutagenesis of the hemagglutinin of influenza virus. *J. Cell Biol.* 102:11–23.
37. Schoen, P., L. Leserman, and J. Wilschut. 1996. Fusion of reconstituted influenza virus envelopes with liposomes mediated by streptavidin/biotin interactions. *FEBS Lett.* 390:315–318.
38. Stegmann, T., I. Bartoldus, and J. Zumbrunn. 1995. Influenza hemagglutinin-mediated membrane fusion: influence of receptor binding on the lag phase preceding fusion. *Biochemistry.* 34:1825–1832.
39. White, J., J. Kartenbeck, and A. Helenius. 1982. Membrane fusion activity of influenza virus. *EMBO J.* 1:217–222.
40. Niles, W. D., and F. S. Cohen. 1993. Single event recording shows that docking onto receptor alters the kinetics of membrane fusion mediated by influenza hemagglutinin. *Biophys. J.* 65:171–176.
41. Wharton, S. A., J. J. Skehel, and D. C. Wiley. 1986. Studies of influenza hemagglutinin-mediated membrane fusion. *Virology.* 149:27–35.
42. Sheetz, M. P. 1983. Membrane skeletal dynamics: role in modulation of red cell deformability, mobility of transmembrane proteins, and shape. *Semin. Hematol.* 20:175–188.
43. Krumbiegel, M., A. Herrmann, and R. Blumenthal. 1994. Kinetics of the low pH-induced conformational changes and fusogenic activity of influenza hemagglutinin. *Biophys. J.* 67:2355–2360.
44. Efron, B., and R. Tibshirani. 1993. An Introduction to the Bootstrap, Vol. 57. CRC Press, Boca Raton, FL.
45. Lentz, B. R., and J. K. Lee. 1999. Poly(ethylene glycol) (PEG)-mediated fusion between pure lipid bilayers: a mechanism in common with viral fusion and secretory vesicle release? *Mol. Membr. Biol.* 16:279–296.
46. Lee, J., and B. R. Lentz. 1997. Evolution of lipidic structures during model membrane fusion and the relation of this process to cell membrane fusion. *Biochemistry.* 36:6251–6259.
47. Gillespie, D. T. 1976. General method for numerically simulating stochastic time evolution of coupled chemical reactions. *J. Comput. Phys.* 22:403–434.
48. Massey, F. J. 1951. The Kolmogorov-Smirnov test for goodness of fit. *J. Am. Stat. Assoc.* 46:68–78.
49. Smirnov, N. 1948. Table for estimating the goodness of fit of empirical distributions. *Ann. Math. Stat.* 19:279–281.
50. Bar Massada, A., and Y. Carmel. 2008. Incorporating output variance in local sensitivity analysis for stochastic models. *Ecol Model.* 213:463–467.
51. Böckmann, R. A., A. Hac, …, H. Grubmüller. 2003. Effect of sodium chloride on a lipid bilayer. *Biophys. J.* 85:1647–1655.
52. Pabst, G., A. Hodzic, …, P. Laggner. 2007. Rigidification of neutral lipid bilayers in the presence of salts. *Biophys. J.* 93:2688–2696.
53. Floyd, D. L., S. C. Harrison, and A. M. van Oijen. 2010. Analysis of kinetic intermediates in single-particle dwell-time distributions. *Biophys. J.* 99:360–366.
54. Cohen, F. S., and G. B. Melikyan. 2004. The energetics of membrane fusion from binding, through hemifusion, pore formation, and pore enlargement. *J. Membr. Biol.* 199:1–14.
55. Kuzmin, P. I., J. Zimmerberg, …, F. S. Cohen. 2001. A quantitative model for membrane fusion based on low-energy intermediates. *Proc. Natl. Acad. Sci. USA.* 98:7235–7240.
56. Chizmadzhev, Y. A. 2004. The mechanisms of lipid-protein rearrangements during viral infection. *Bioelectrochemistry.* 63:129–136.
57. Kozlovsky, Y., and M. M. Kozlov. 2002. Stalk model of membrane fusion: solution of energy crisis. *Biophys. J.* 82:882–895.
58. Huang, Q., R. P. Sivaramakrishna, …, A. Herrmann. 2003. Early steps of the conformational change of influenza virus hemagglutinin to a fusion active state: stability and energetics of the hemagglutinin. *Biochim. Biophys. Acta.* 1614:3–13.
59. Axelrod, D., D. E. Koppel, …, W. W. Webb. 1976. Mobility measurement by analysis of fluorescence photobleaching recovery kinetics. *Biophys. J.* 16:1055–1069.
60. Bernstein, D. 2005. Simulating mesoscopic reaction-diffusion systems using the Gillespie algorithm. *Phys. Rev. E Stat. Nonlin. Soft Matter Phys.* 71:041103.
61. Arjunan, S. N., and M. Tomita. 2010. A new multicompartmental reaction-diffusion modeling method links transient membrane attachment of *E. coli* MinE to E-ring formation. *Syst. Synth. Biol.* 4:35–53.
62. Klein, A. M., V. Nikolaidou-Neokosmidou, …, B. D. Simons. 2011. Patterning as a signature of human epidermal stem cell regulation. *J. R. Soc. Interface.* 8:1815–1824.

SUPPORTING MATERIAL FOR

Stochastic fusion simulations and experiments suggest passive and active roles of hemagglutinin during membrane fusion

Donald W. Lee,* Vikram Thapar,* Paulette Clancy and Susan Daniel[#]

School of Chemical and Biomolecular Engineering

Cornell University, Ithaca, NY 14853

Overview

This supporting material provides additional details on prior literature, microfluidic preparation, fusion assay setup, fluorescence recovery after photobleaching (FRAP) experiments, extents of fusion, a list of species used in simulation, calculation of "hopping rate" for species diffusion in the simulation, refining the k_{bend} values, the fusible unit species tested by simulation, our simulation algorithm, flow chart of simulation strategy, and a sensitivity analysis of slopes of log V_{max} vs log [$HA_{1,2}$] plots.

Summary of literature work

The minimal number of HA trimers necessary for membrane fusion, w, and the minimal number of activated HA trimers required, q, have been debated for more than two decades. Table S1 is a summary of past work related to this topic, together with the authors' original hypothesis or conclusions for suitable values of w and q. Each work has been classified according to the experimental approach used to determine w and q, as described in the table caption. Note that many previous studies did not consider w and q as separate parameters, which is why w and q often appear as the same value in the table.

Year	Authors	Approach	*w*	*q*	Fitting Method	Source of HA trimer	Fusion Exp. or Simulation
1986	Gibson et al.	Var F	1	1	Multiple-Hit-Multiple-Target Model	A/PR/8/34 (H1N1)	Virus-Vesicle
1987	Bundo-Morita et al.	Var F	1	1	Multiple-Hit-Multiple-Target Model	A/PR/8/34 (H1N1)	Virus-Vesicle
1990	Ellens et al.	Var FB	2-5	2-5	N/A	A/Japan/305/57 (H2N2)	Cell-Vesicle
1990	Stegmann et al.	Const. FB	> 1	> 1	N/A	X-31 A/Aichi/68 (H3N2)	Virus-Vesicle
1996	Danieli et al.	Var FB	3-4	3-4	Hill Equation	A/Japan/305/57 (H2N2)	Cell-Cell
1996	Blumenthal et al.	Const FB	6	6	Power Law	A/Japan/305/57 (H2N2)	Cell-Cell
2000	Günther-Ausborn et al.	Var F	1	1	$V_{initial} = k[HA_{1,2}]^q$	A/Shangdong (H3N2) X-47 (H3N2)	Virosome-Cell
2000	Bentz	Var FB + Const FB	> 8	2-3	Mass Action Kinetic Model	A/Japan/305/57 (H2N2)	Cell-Cell
2001	Schreiber et al.	Var FB + Const FB	3	3	Simulation	A/Japan/305/57 (H2N2)	Cell-Cell
2006	Imai et al.	Var F Var FB	1 > 1	1 > 1	$V_{max} = k[HA_{1,2}]^q$	A/PR/8/1934 (H1N1)	Virosome-Cell
2008	Floyd et al.	Const FB	3	3	Gamma Distribution	X-31 A/Aichi/68 (H3N2)	Virus-SLB
2011	Dobay et al.	Const FB	6	3	Simulation	A/PR/8/1934 (H1N1) X-31 A/Aichi/68 (H3N2)	Virus-SLB
2012	Costello et al.	Const FB	≤ 2	≤ 2	Gamma Distribution	X-31 A/Aichi/68 (H3N2)	Virus-SLB
2013	Ivanovic et al.	Const FB	3-4	3-4	Gamma Distribution & Simulation	A/Udorn/62 (H3N2) X-31 A/Aichi/68 (H3N2)	Virus-SLB
2013	Lee et al. (this work)	Var F + Var FB + Const FB	3	1	Simulation	A/PR/8/1934 (H1N1) X-31 A/Aichi/68 (H3N2)	Virosome-Cell Virus-SLB

TABLE S1 Chronological list of experiments related to determining *w* or *q*. Variable F (var F) varies the fraction of fusogenic HA trimers at a constant total HA density. Variable FB (var FB) varies the total density of fusogenic HA trimers. Constant FB (const FB) does not vary HA density and extracts *w* or *q* by fitting fusion lag time data to statistical models. The reported *w* and *q* values from listed studies were interpreted from the original references and not obtained through simulations performed in this work.

Microfluidic preparation

The microfluidic devices used for fusion experiments were prepared according to the following procedure. Glass coverslip slides (No. 1.5 thickness) [VWR, Radner, PA] were cleaned for 10 min using a piranha solution consisting of 45 mL of 50% hydrogen peroxide [Sigma-Aldrich, St. Louis, MO] and 105 mL of sulfuric acid [VWR, Radner, PA]. Cleaned glass slides were rinsed and stored in deionized water. A polydimethylsiloxane (PDMS) [Dow Corning, Midland, MI] mold of microfluidic channels was prepared using a patterned silica wafer made through photolithography. The microfluidic channel dimensions are 135 μm wide, 75 μm deep, and 1.5 cm long. A glass slide and PDMS mold were annealed together after a 30-second oxygen plasma cleaning step. Tygon tubes (0.02”ID x 0.06”OD) [Saint-Gobain Performance Plastic, Worcester, MA] were attached to the microfluidic device to facilitate the loading of various solutions into the channels. The microfluidic device is shown in Fig. S1.

Images of fusion assay and sample hemifusion event

Fig. S1 shows a picture of the microfluidic device and schematic drawing of the fusion assay setup. A sample image sequence of a fusing virus is also shown. The intensity traces of the membrane dye (R18) in the virus and the acid-sensitive membrane dye (Oregon Green) in the target membrane are used to determine the hemifusion lag time for an individual virion.

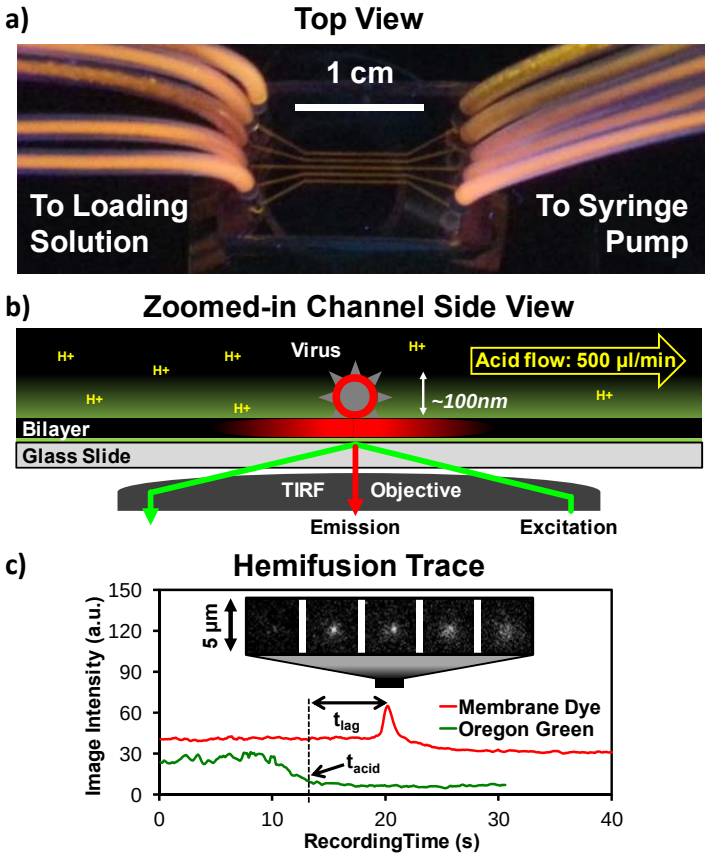

FIGURE S1 Virus fusion assay setup and sample hemifusion trace. (a) Photo of a typical microfluidic device. Channels were filled with fluorescent dye for visualization purposes. (b) Schematic diagram of a microfluidic channel used in experiments. A dye-labeled virus is shown fusing to a supported lipid bilayer (SLB) upon an acid trigger, inside a channel. Total internal reflection fluorescence (TIRF) microscopy is used to observe the fusion events. (c) Sample virus fusion images and hemifusion trace showing how the hemifusion lag time, t_{lag}, is determined.

Fluorescence recovery after photobleaching (FRAP) experiments

The mobility of the target membranes were determined using FRAP. The target membranes were labeled with R18 membrane fluorophores by adding 0.5 µL of 1.8 mM R18 in ethanol solution to 500 µL of lipid A or lipid B vesicle solutions. The solutions were sonicated for 30 min before loading them into microfluidic channels to form supported lipid bilayers (SLBs), which were allowed to form over the course of 20 min. Channels with SLBs were rinsed with citric acid buffer set at pH 3.0, 3.5, 4.0, or 4.5. The bilayer was illuminated with a 561 nm

wavelength light source. A 16 μm-diameter circular area in the bilayer was photobleached with a 5 mW, 561 nm wavelength Gaussian laser for 3 seconds. Video images of the bilayer were recorded before and after photobleaching, and the mean intensity of the bleached spot over time was measured. Another area that has not been photobleached, the reference spot (see Fig. S2), was monitored to correct for global photobleaching caused by the microscope light source. The normalized mean intensity of the photobleached region, $f_k(t)$, was determined according to the following equation:

$$f_k(t) = \frac{[F_k(t) - F_c(t)] - [F_k(0) - F_c(0)]}{[F_k(-\infty) - F_c(-\infty)] - [F_k(0) - F_c(0)]}$$

where $F_k(t)$ and $F_c(t)$ are the fluorescence intensities at time t of the bleached and reference spot, respectively. The time immediately after photobleaching is $t = 0$, and the time before photobleaching is $t = -\infty$. The methods of Axelrod et al. (1) were used to fit the fluorescence recovery data and extract the characteristic time for diffusion, t_d, for a bleach spot made from a Gaussian laser. The diffusion coefficient was calculated as $D = r^2/(4t_d)$, where r is the radius of the laser beam at e^{-2} laser intensity height. D values for R18 fluorophores in SLB A are shown in Fig. 5b of the main report.

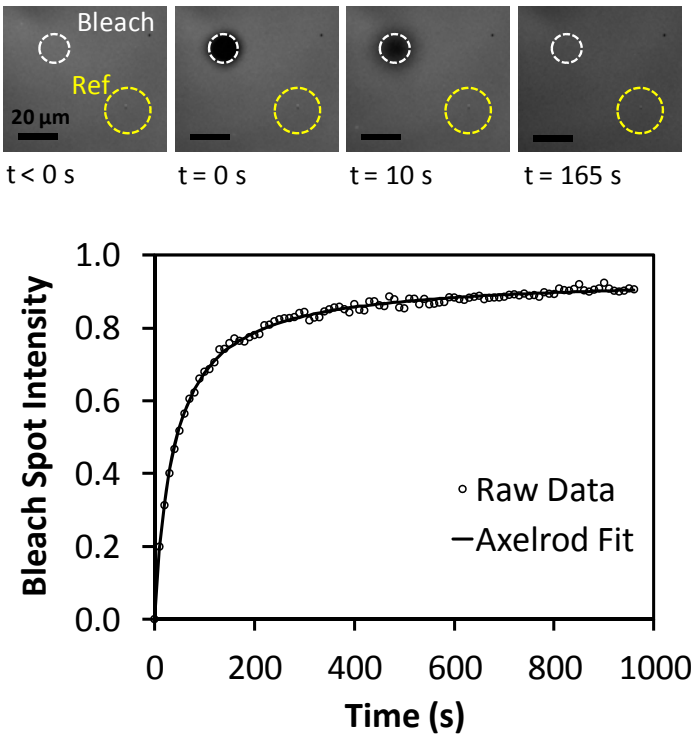

FIGURE S2 A representative FRAP recovery curve used to determine diffusion coefficient in supported bilayers. (Top) Image sequence of a R18-labeled supported lipid bilayer with LPC lipid (SLB B) at pH 4.5. The mean intensity of the photobleached circular region (white dotted circle) is tracked and compared with a reference region (yellow dotted circle) that has not been photobleached. (Bottom) the normalized intensity of the bleached spot is plotted with time and fitted to the diffusion equation derived by Axelrod et al. (1) to extract the characteristic time for diffusion, t_d. For this example, the bleach spot radius, r, is 8.13 µm and t_d is 36 s. The calculated D is 0.46 µm^2/s.

Extents of fusion of experimental data

The fraction of bound viruses that fused was tracked to verify that protein denaturation and subsequent loss of function due to acidification is negligible in the range of pH employed in these studies. An in-house particle counting program was developed in MATLAB to detect and count fluorescently-labeled virus particles by identifying high-intensity spots that have a circular morphology. Extent of fusion is defined as the number of viruses that fused divided by the total number of viruses observed. Fig. S3 show the resulting extents of fusion at various pH conditions for triggering fusion. The consistent fusion extents across the tested pH range suggest that the virions were similarly functional across the experiments, and also that acid-induced

denaturation of HA trimers is not occurring across the pH range. This result is also in agreement with studies by Doms et al. in 1985 (2), who investigated acid-induced denaturation of HA trimers.

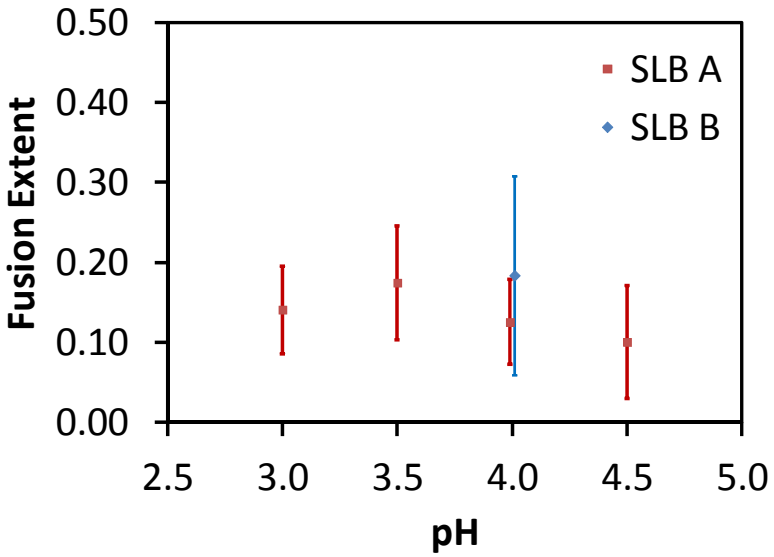

FIGURE S3 Extent of fusion for the X31 virus as the pH is varied in the range 3.0-4.5. The extent of fusion in this range is essentially the same within the uncertainty in the data.

List of species used in simulation

Table S2 is a list of all species used in the simulation, with their description and allowable locations in the simulation space. Species that are physically associated with both the viral and host membrane are only allowed in the contact area region.

Outside the contact area, only HA_0, $HA_{1,2}$, $HA_{1,2}^*$, and *R* are mobile species. Inside the contact area, any HA trimers that are physically interacting with the target membrane or receptor are treated as immobile species. Unbound HA_0 and unbound *R* remain mobile inside the contact area. Table S2 summarizes the mobility of species.

Symbol	Description	Allowed Location	Mobility
R	Sialic acid receptor	Anywhere	Mobile
$HA_{1,2}$	Fusogenic $HA_{1,2}$ trimer	Anywhere	Mobile
HA_0	Non-fusogenic HA_0 trimer	Anywhere	Mobile
$HA_{1,2}$-*R* HA_0-*R* $HA_{1,2}$*-*R*	An HA trimer that is bound to R	Contact Area	Immobile
$HA_{1,2}$*	Conformationally changed $HA_{1,2}$	Anywhere	Immobile inside contact area. Mobile elsewhere.
Fusible Unit	An arrangement of HA trimers that can bend the target bilayer.	Contact Area	N/A
Bent Complex	A bent state of the target bilayer, which precedes hemifusion.	Contact Area	Immobile
Hemifusion Stalk	A merged state of the virus and target bilayer.	Contact Area	Immobile

TABLE S2 Summary of the species involved in the simulations.

Calculation of "hopping rate" for species diffusion in the simulation

The only diffusive species in our simulation are receptors, *R*, and HA trimers, HA_0, $HA_{1,2}$, or $HA_{1,2}^*$. A diffusion event is defined as the migration of a molecule from one grid element to a neighboring grid element. This is modeled as a unimolecular reaction (3), where the hopping rate parameter is related to the macroscopic diffusion coefficient *D* through the relation $k_{diff} = nD/h^2$, where *h* is the center to center distance between two adjacent grid elements, and *n* is 2/3 for a hexagonal lattice system (4-5). The diffusion coefficients for HA and glycoprotein receptor were estimated from existing FRAP experiments by Danieli et al. (6) and Sheetz (7), respectively. The hopping rate for HA, $k_{diff,HA}$, was calculated as 740 s^{-1}, while that for the glycoprotein is 74 s^{-1}. We assumed that the viruses studied by Imai et al. were attached to the glyocoprotein on the ghost red blood cell membranes. As for our own experiments, the viruses were bound to a different receptor called GD_{1a}, a glycolipid with sialic acid groups. The diffusion coefficient for $GD_{1a}$was estimated at 1 $\mu m^2/s$ based on the diffusion coefficient of the

lipid fluorophore, R18. However, the calculated hopping rate for GD_{1a}, $k_{diff,R}$,is 24,700 s^{-1}, which is many orders of magnitude greater than other rate parameters in the simulation. The simulation algorithm (discussed in detail below) will simulate each reaction event according to their reaction propensities, and therefore GD_{1a} diffusion would dominate the most of the simulation processing power. To prevent this from happening, we have capped $k_{diff,R}$ for GD_{1a} at 2000 s^{-1}.

Refining k_{bend} values

To refine the k_{bend} values starting with $k_{bend,approx}$, the bootstrap method (8) is used. In this method, the k_{bend} parameter is varied at 10 evenly spaced values in the interval [$0.8k_{bend,approx}$, $1.2k_{bend,approx}$] in which 3000 simulations are performed for each k_{bend} value. In one iteration of refinement, 500 random lag times from each distribution for each k_{bend} value are compared to the actual lag time distribution through a KS test. The simulated distribution with the smallest KS statistic (D_{test}) is determined, and the k_{bend} value for that distribution is stored. This iteration is performed for a total of 6 times to find the mean and standard deviation of these stored k_{bend} values. In the main text, any k_{bend} values with their error bars reported have been refined using this procedure.

Fusible unit species tested by simulation

A fusible unit is defined by an arrangement of HA trimers in adjacent grid elements. At least q number of HA trimers must be pH-activated and the relative locations of the pH-activated and un-activated HA trimers do not matter within the fusible unit perimeter, highlighted by a thick blue line in Fig. S4. Other configurations of fusible units for different combinations of w and q are shown below in Fig. S4.

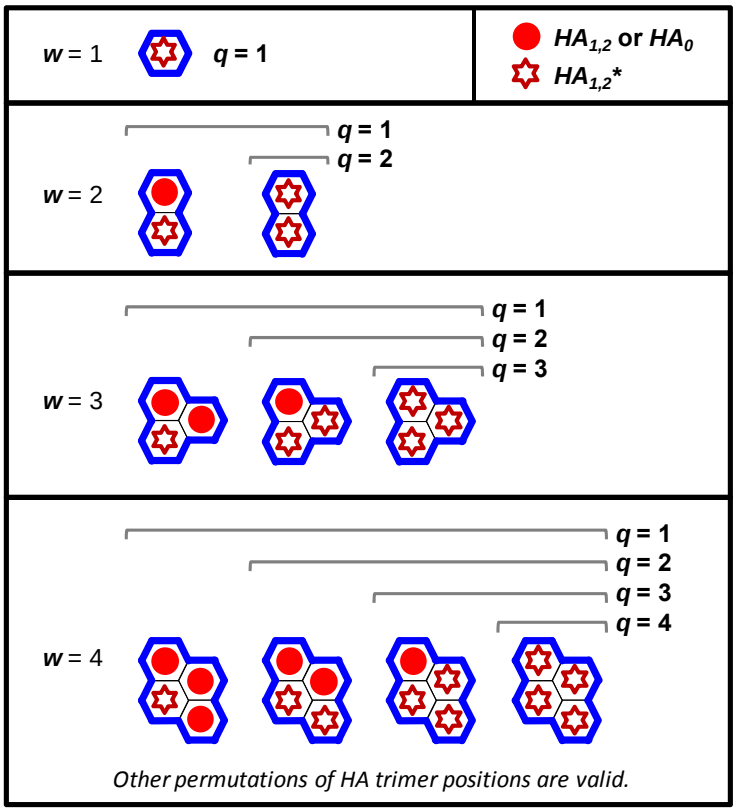

FIGURE S4 Fusible unit species studied in this simulation. A fusible unit is defined as a localized group of hexagonal lattice grid elements that contain *w* HA trimers, regardless of conformational state, and at least *q* activated HA trimers. Permutations of the positions of HA trimers within the blue fusible unit perimeter do not matter when defining a fusible unit species.

Simulation algorithm

Stochastic fusion simulations are performed using the following iterative procedure.

1) Initialize the system at time $t = 0$, which corresponds to the time at which the system is acidified.

2) Calculate the propensity, $a(t)$, of all molecular events using the relation $a_i(t) = k_i G_i(t)$, where k_i is the rate parameter of event i and $G_i(t)$ is the number of species involved, which

here would be the number hexagonal lattice grid elements (or groups of elements) containing those species.

3) Select a random molecular event j by finding the minimum j value that satisfies $\frac{\sum_{j'=1}^{j} a_{j'}(t)}{a_0(t)} \geq r_1$, where $a_0(t)$ is the total propensity of all events and r_1 is a uniform random number in an interval [0,1].

4) Calculate time step, τ, using the relation $\tau = \frac{1}{a_0} \ln\left(\frac{1}{r_2}\right)$, where r_2 is a uniform random number in an interval [0,1].

5) Advance the simulated time, t, by τ and update the population/location of species in the simulation based on the chosen event.

6) Repeat steps 2 through 5 until a terminating event occurs. Our termination events were the formation of a hemifusion stalk species or a simulated time of t = 5 min.

Flow chart of simulation strategy

The flow chart in Fig. S5 summarizes the strategy used to determine the unknown parameters (w, q, and k_{bend}) and also to validate the model. More details are provided in the Main Text in the section titled "Strategy Overview for Determining w and q."

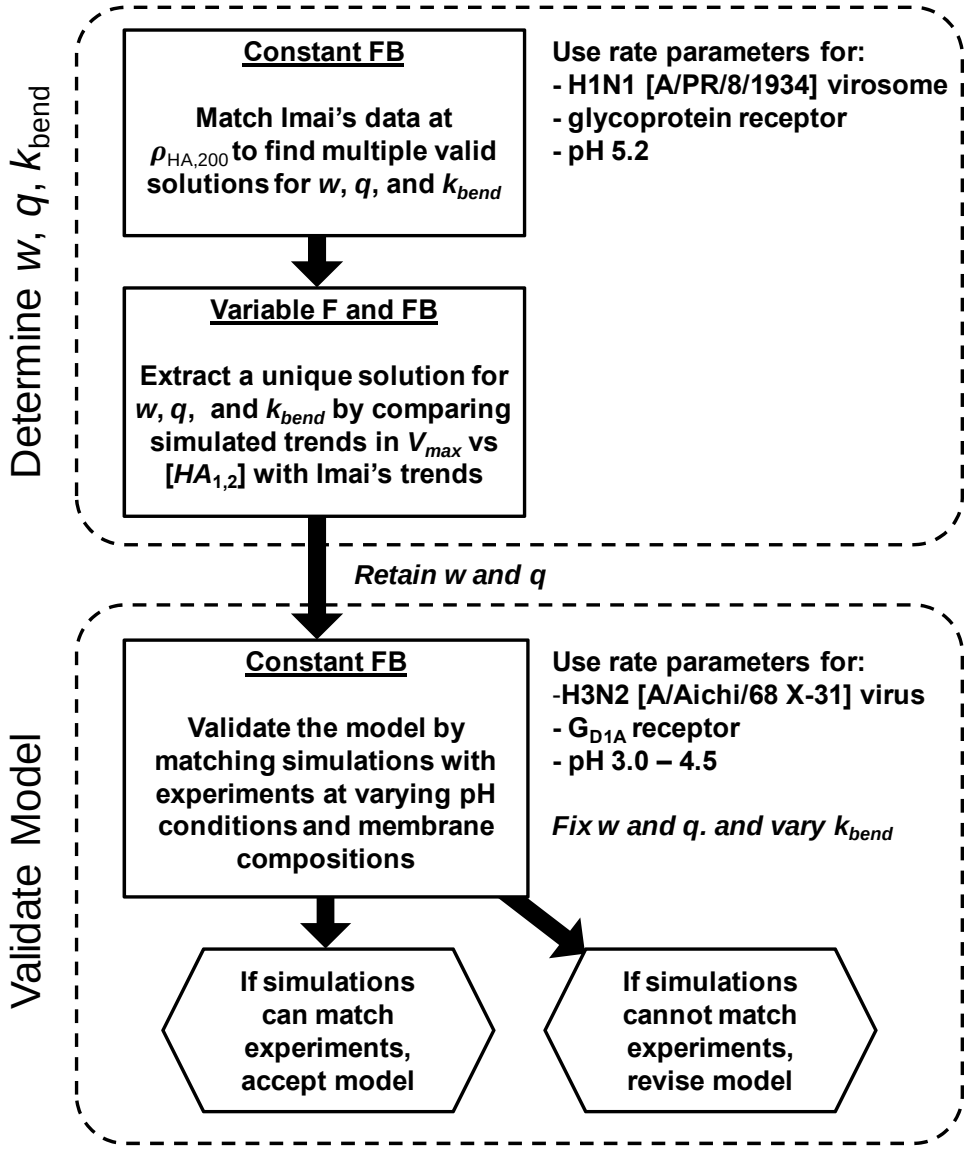

FIGURE S5 Flow diagram of the simulation process used to determine values for k_{bend}, w, and q.

Sensitivity analysis of slopes of log V_{max} vs log [$HA_{1,2}$] plots

We performed two types of sensitivity analysis to illustrate the robustness of our model in determining w and q. In the first analysis, we repeated the Variable F and FB simulations at two other contact areas to ensure that w and q values were dependent on our original choice of contact area size. The slopes of plots of log V_{max} vs log [$HA_{1,2}$] for both Variable F and FB simulations did not change significantly for 8×8, 10×10, and 14×14 grid sizes for the contact

area. Thus, our conclusions regarding optimal w and q values are not affected by the choice of contact area size (Fig. S6). We note that the choice of contact area size does alter the k_{bend} values obtained by matching with Imai et al.'s distribution at $\boldsymbol{\rho}_{\mathrm{HA},200}$. A larger contact area increases the rate of fusion, which is compensated by a lower k_{bend} value in order to match experimental data. We thus emphasize that our numerical rate value reported for k_{bend} is based on the contact area being 2338 nm^2 (which is equivalent to 10x10 hexagonal grid elements), and that it scales directly with contact area size.

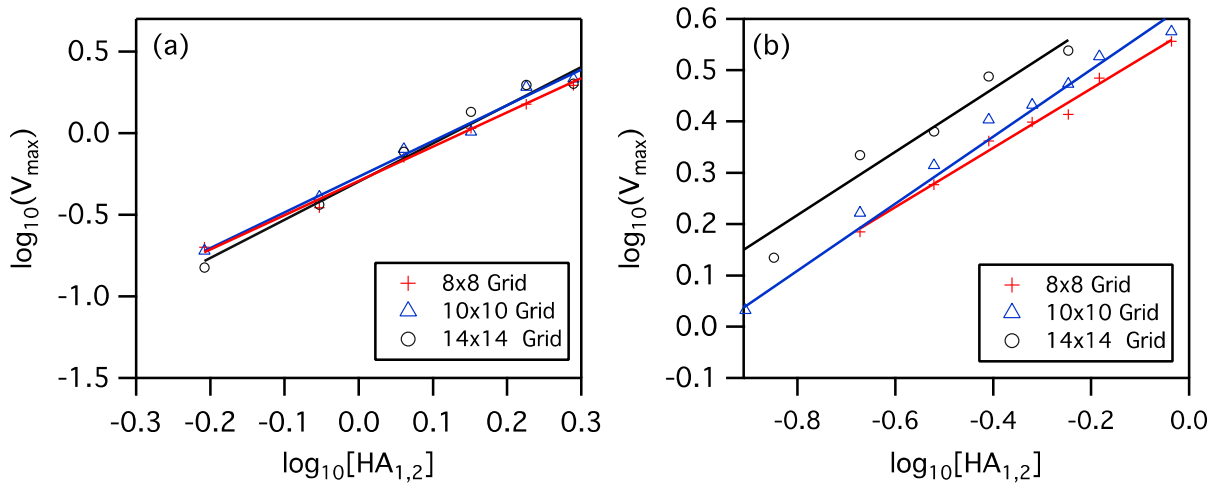

FIGURE S6 Insensitivity of slopes of log V_{max} vs log [$HA_{1,2}$] to choice of contact area size, for w = 3, q = 1, and k_{act} = 0.067 s^{-1}. (a) Results from Variable FB simulations. The slopes of the best-fit lines are 2.09 (r^2 = 0.99), 2.19 (r^2 = 0.99) and 2.34 (r^2 = 0.99) for contact area sizes of 8×8, 10×10, and 14×14 grid elements, respectively. (b) Results from Variable F simulations. The slopes of the best-fit lines are 0.58 (r^2 = 0.98), 0.65 (r^2 = 0.99) and 0.62 (r^2 = 0.97) for contact area sizes of 8×8, 10×10, and 14×14 grid elements, respectively. The HA density, [$HA_{1,2}$], has been converted to its corresponding mass ratio of HA to lipid in this plot to be consistent with Imai et al.'s studies (9). The $k_{bend,\ approx}$ values determined from the fits are 0.078 s^{-1}, 0.05 s^{-1}, and 0.0255 s^{-1} for the 8x8, 10x10, and 14x14 contact area sizes, respectively.

In the second analysis, we repeated the Variable F and FB simulations at another k_{act} value to ensure that this parameter did not change our choice of values for w and q. We performed this analysis because we do not know the rate of conformational change for the HA

trimers in the H1N1 influenza virus used by Imai et al. (9). We began by using a value for k_{act} of 0.067 s^{-1}, which is the HA activation rate for X31 virus (H3N2) at pH 5.2, the pH value used by Imai et al. For a second value, we chose an arbitrary k_{act} value of 0.01 s^{-1}. Variable F and FB simulations were run for both cases of k_{act} using the same procedure described in the main manuscript. Despite an almost order of magnitude difference in k_{act}, the slopes of the log V_{max} vs log [$HA_{1,2}$] plots did not change, as shown in Fig. S7. In the main manuscript, we also showed that using a k_{act} value of 5.2 s^{-1} did not require us to change w and q when studying fusion kinetics at pH values below 4.5 and with different membrane compositions. Taken together, these results suggest that w and q is insensitive to the choice of k_{act} value, at least within the range of 0.01 and 0.067 s^{-1} studied here.

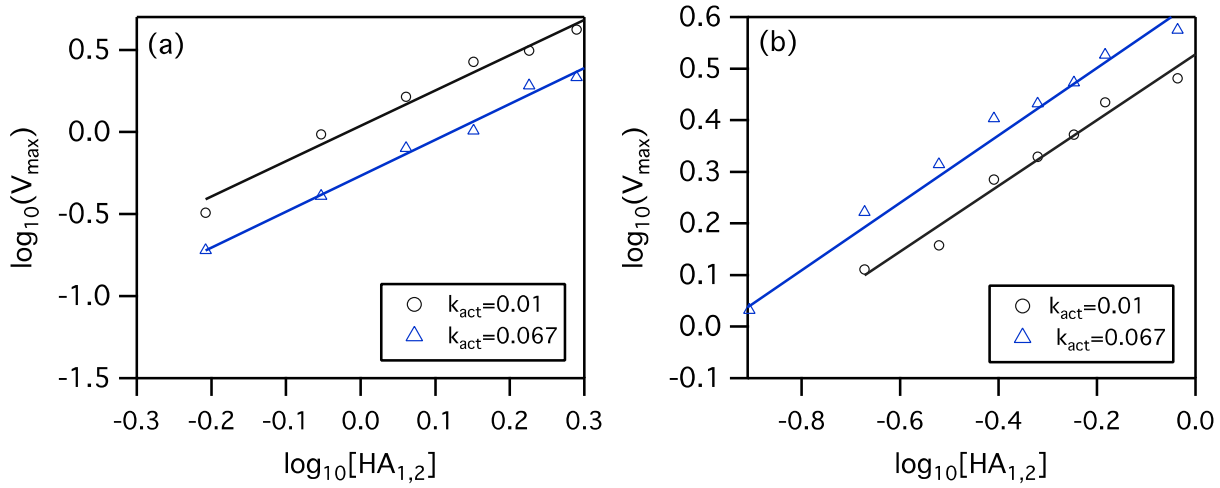

FIGURE S7 Insensitivity of slopes of log V_{max} vs log [$HA_{1,2}$] to the choice of k_{act}, for w = 3, q = 1, and contact area = 10x10 grid size (2338 nm^2). a) Results from Variable FB simulations. The slopes of the best-fit lines are 2.19 (r^2 = 0.99) and 2.23 (r^2 = 0.98) when k_{act} is 0.067 and 0.01 s^{-1}, respectively. b) Results from Variable F simulations. The slopes of the best-fit lines are 0.65 (r^2 = 0.99) and 0.62 (r^2 = 0.98) when k_{act} is 0.067 and 0.01 s^{-1} respectively. The HA density, [$HA_{1,2}$], has been converted to its corresponding mass ratio of HA to lipid in this plot to be consistent with Imai et al. (9). The $k_{bend,\ approx}$ values from the fits are 0.28 and 0.05 $s^{-1}$for k_{act} values of 0.01 and 0.067 s^{-1}, respectively.

SUPPORTING REFERENCES

1. Axelrod, D., D.E. Koppel, J. Schlessinger, E. Elson, and W.W. Webb. 1976. Mobility measurement by analysis of fluorescence photobleaching recovery kinetics. BIOPHYS J. 16:1055-1069.
2. Doms, R.W., A. Helenius, and J. White. 1985. Membrane fusion activity of the influenza virus hemagglutinin. The low pH-induced conformational change. J BIOL CHEM. 260:2973-2981.
3. Bernstein, D. 2005. Simulating mesoscopic reaction-diffusion systems using the Gillespie algorithm. PHYS REV E. 71:041103.
4. Arjunan, S. and M. Tomita. 2010. A new multicompartmental reaction-diffusion modeling method links transient membrane attachment of E. coli MinE to E-ring formation. SYST SYNTH BIOL. 4:35-53.
5. Klein, A.M., V. Nikolaidou-Neokosmidou, D.P. Doupé, P.H. Jones, and B.D. Simons. 2011. Patterning as a signature of human epidermal stem cell regulation. J ROY SOC INTERFACE. 8:1815-1824.
6. Danieli, T., S.L. Pelletier, Y.I. Henis, and J.M. White. 1996. Membrane fusion mediated by the influenza virus hemagglutinin requires the concerted action of at least three hemagglutinin trimers. J CELL BIOL. 133:559-569.
7. Sheetz, M.P. 1983. Membrane skeletal dynamics: role in modulation of red cell deformability, mobility of transmembrane proteins, and shape. SEMIN HEMATOL. 20:175-188.
8. Efron, B. and R. Tibshirani, *An introduction to the bootstrap*. Vol. 57. 1993: CRC press.
9. Imai, M., T. Mizuno, and K. Kawasaki. 2006. Membrane fusion by single influenza hemagglutinin trimers. J BIOL CHEM. 281:12729-12735.